ACS APPLIED MATERIALS & INTERFACES

Research Article

www.acsami.org

Quantitative Understanding of pH- and Salt-Mediated Conformational Folding of Histidine-Containing, β-Hairpin-like Peptides, through Single-Molecule Probing with Protein Nanopores

Loredana Mereuta,[†] Alina Asandei,[‡] Chang Ho Seo,[§] Yoonkyung Park,[∥] and Tudor Luchian*[,†]

[†]Department of Physics, Alexandru I. Cuza University, Iasi 700506, Romania

[‡]Department of Interdisciplinary Research, Alexandru I. Cuza University, Iasi 700506, Romania

[§]Department of Bioinformatics, Kongju National University, Kongju 182, South Korea

[∥]Research Center for Proteineous Materials, Chosun University, Gwangju 375, South Korea

Supporting Information

ABSTRACT: Inter-amino acid residues electrostatic interactions contribute to the conformational stability of peptides and proteins, influence their folding pathways, and are critically important to a multitude of problems in biology including the onset of misfolding diseases. By varying the pH and ionic strength, the inter-amino acid residues electrostatic interactions of histidine-containing, β-hairpin-like peptides alter their folding behavior, and we studied this through quantifying, at the unimolecular level, the frequency, dwell-times of translocation events, and amplitude of blockades associated with interactions between such peptides and the α-hemolysin (α-HL) protein. Acidic buffers were shown to dramatically decrease the rate of peptide capture by the α-HL protein, through the interplay of enthalpic and entropic contributions brought about on the free energy barrier, which controls the peptides−α-HL association rate. We found that in acidic buffers, the amplitude of the blockage induced by an α-HL, β-barrel-residing peptide is smaller than the value seen at neutral pH, and this supports our interpretation of the pH-induced change in the conformation of the peptide, which behaves as a less-stable hairpin at acidic pH values that obstructs, to a lesser extent, the protein pore. This is also confirmed by the fact that the dissociation rate of such model peptide from the α-HL's β-barrel is higher at acidic, as compared to neutral, pH values. Experiments performed in low-salt buffers revealed the dramatic decrease of the peptide capture rate by the α-HL protein, most likely caused by the increase in the radius of counterions cloud around the peptide that hinders peptide partition into the α-barrel, and histidines protonation at low pH bolsters this effect. Reduced electrostatic screening in low-salt buffers, at neutral pH, leads to a decrease in peptides effective cross-sectional areas and an increase of their mobility inside the α-HL pore, due most likely to the chain stretching augmentation, via increased inter-residues electrostatic interactions.

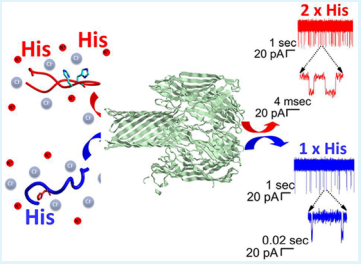

KEYWORDS: *protein nanopore, single-molecule electrophysiology, peptide folding, histidine*

INTRODUCTION

A wide selection of biological phenomena, such as enzymatic processes, protein aggregation, and peptide folding and misfolding, proceed through a pH-dependent conformational dynamics, and aggregation of amyloidogenic proteins and peptides is associated with the onset of several diseases, including Alzheimer's disease, Parkinson's disease, Huntington's disease, and type II diabetes mellitus.[1] It is established that electrostatic interactions among the charged moieties of ionizable amino acid residues can contribute significantly to the conformational stability of proteins, and they are responsible for the salt and pH dependence of peptide and protein conformational stability.[2] The accepted paradigm states that stability, solubility, and spatial structure of peptides and proteins, and thus their ability to recognize and interact with other molecules, depend on the ionic strength through the screening effect of the long-range electrostatic interactions among charged moieties of ionizable residues, and concentration of hydrogen ions in the electrolyte, which modulates the net charge on protonable amino acid residues. Various macroscopic techniques, such as circular dicroism, NMR, EPR, Raman spectroscopy, and molecular dynamics simulations, were implicated to investigate in bulk and at mesoscopic scales the influence of salts on the conformational equilibrium of peptides and proteins. It was established that pH and electrostatic screening significantly influence the free energy landscape of peptides and modulate the stability of various conformations,[2−6] and an elevated ionic strength favors more compact states of the conformational equilibrium of peptides, as their radius of gyration decreases as the salt concentration increases.[7] Intramolecular folding events of β-hairpin peptides are triggered by the presence of salt, as the

Received: May 20, 2014
Accepted: July 18, 2014
Published: July 18, 2014

Table 1. Biophysical Properties of the CAMA 1 and CAMA 3 Peptides

peptides	sequence	length (AA)	molecular weight (g/mol)	hydrophobicity[a] (%)	effective charge |e⁻|	
					pH = 7	pH = 4.5
CAMA 1	KWKLFKKIGIGK*H*FLSAKKF-NH_2	20	2405.0	45	8	9
CAMA 3	KWKLKK*H*IGIGK*H*FLSAKKF-NH_2	20	2394.9	40	8	10

[a]Calculated with the help of GenScript Peptide Property Calculator.[60]

unfolded states encountered in the absence of salt at neutral pH, change to a β-hairpin-like conformation when the ionic strength is increased, and this was explained as a direct consequence of the electrostatic screening between charged amino acids within the peptide.[8]

The nanopore-based technology stands currently as an area of tremendous potential for the purpose of sampling the conformational subspaces associated with folding transitions of peptides and proteins, not accessible in bulk measurements.[9−16] The underlying principle is that peptides and protein capture, entry and subsequent translocations through nanopores, which are all characterized at the single molecule level by modulations of the individual nanopores-mediated, current blockage events, depend upon their physicochemical and topological features. The potential of this approach was revealed initially by the possibility of sensing single polymers in bulk,[17] proof-of-concept demonstration to detect RNA and DNA molecules,[18] and unique capability of studying various chemistries at high resolution.[19−26] Among other particular attributes, nanopores possess the exquisite ability of revealing information about the volume of individual molecules, which is of paramount importance for studying protein folding,[27−30] and as concrete examples in this respect, single protein unfolding transitions were amenable to investigation in the presence of denaturing agents,[31,32] or extrinsic factors such as temperature[33] and electric fields.[34,35]

Coupled with electrical recordings in artificial lipid membranes, the α-hemolysin (α-HL) protein secreted by *Staphylocous aureus*[36] is being widely used for single-molecule, protein nanopore-based studies. The α-HL is structurally stable over a wide range of experimental conditions including extreme pH, temperature, and salt variations;[37−39] its behavior is reproducible, and post-translational mutagenesis or chemical modifications makes it an acclaimed tool in the field of molecular sensing and elucidation of molecular details of protein and peptide unfolding or translocation through nanopores.[28,40−47] In particular, it has been established the potential of α-HL to reveal microscopic insights about modulatory effects induced by certain divalent metals or small molecules on peptides and proteins folding processes.[48−54]

In recent work from our laboratories, we focused on 20 amino acids short peptides whose two critically positioned glycine residues at positions 9 and 11, separated by one isoleucine at position 10, favor free states where the peptide assumes a heterogeneous, floppy kinked, β-hairpin-like shape, and in the narrow space provided by the α-HL's β-barrel and vestibule, such peptides' β-hairpin-like conformation is further stabilized by inter-residue hydrogen bonding.[55] Motivated by the fact that the hairpin-like conformations constitute one of the important factors for the toxicity of peptides and proteins associated with human neurodegenerative disorders,[56,57] and given the remarkable impact of histidine residues in establishing peptides activity,[58] herein we aimed at studying the pH and salt dependence of folding state of histidine-containing, β-hairpin-like peptides, engineered based on the simple scaffold described before.[55]

The underlying idea was that by working under experimental conditions whereby histidine residues assume either the protonation or deprotonation state, and distinct salt concentration, one should be able to modulate the electrostatic interactions within the peptide and therefore tune its folding behavior, which, in the end, alters their propensity to interacting with the α-HL protein. The followed strategy was to record and analyze the frequencies, dwell-times of translocation events, and current amplitude of the blockades associated with interactions between a single α-HL protein and peptides containing one or two histidine residues, in the presence of various salt concentrations, at neutral and acidic pH values, and interpreted differences events parameters in terms of structural changes of peptides.

Our results demonstrate the ability of the α-HL nanopore approach to distinguish between different peptide conformations at the single molecule level, and utility of the technique for the evaluation of salt- and pH-related contribution to the overall folding of histidine-containing peptides, as an attractive approach for tuning peptide folding propensity.

EXPERIMENTAL SECTION

1. Peptides Synthesis. The peptides used in this work (Table 1) were synthesized as described before[55] using the solid phase method with Fmoc (9-fluorenyl-methoxycarbonyl) chemistry.[59] Peptide purification was carried out using preparative high-performance liquid chromatography (HPLC) on a C18 reverse-phase column. The amino acid compositions of the purified peptides were confirmed using an amino acid analyzer (HITACHI 8500A, Japan). The molecular weights of the synthetic peptides were determined using a matrix-assisted laser desorption ionization (MALDI) mass spectrometer (Axima CFR, Kratos Analytical, Manchester, UK).

2. Protein Electrophysiology. Single-molecule electrophysiology experiments were performed as previously described.[43,48] Briefly, membranes were made of 1,2-diphytanoyl-*sn*-glycerophosphocholine (Avanti Polar Lipids, Alabaster, AL) across an orifice with a diameter of ~120 μm punctured on a 25 μm thick Teflon film (Goodfellow, Malvern, MA), which was pretreated with a 1:10 hexadecane/pentane solution (HPLC-grade, Sigma-Aldrich, Germany), and separated the cis (grounded) and trans chambers of the recording cell. The electrolyte used in both chambers contained KCl at different concentration (symmetrical 2 M, 1, or 0.5 M and asymmetrical 2 M_{trans}/0.5 M_{cis}, 0.5 M_{trans}/2 M_{cis}, or 0.1 M_{trans}/2 M_{cis}), buffered in 10 mM *N*-(2-hydroxyethyl)piperazine-*N*′-(2-ethanesulfonic acid (HEPES) (Sigma-Aldrich, Germany) for experiments performed at pH = 7, or 5 mM 2-(*N*-morpholino)ethanesulfonic acid (MES) (Sigma-Aldrich, Germany) for experiments carried out at mildly acidic pH (pH = 4.5). All reagents were of molecular biology purity. After a mechanically stable lipid bilayer was obtained, ~0.5−2 μL of α-hemolysin (α-HL) (Sigma-Aldrich, Germany) was added from a monomeric stock solution made in 0.5 M KCl, to the grounded, cis chamber, under continuous stirring for about 5−10 min. Once the successful membrane insertion of a single α-HL heptamer was attained, and depending on the particular experiment, either CAMA 3 or CAMA 1 peptide was introduced in the trans chamber at a bulk concentration of 30 μM, from a 1 mM stock solution made in distilled

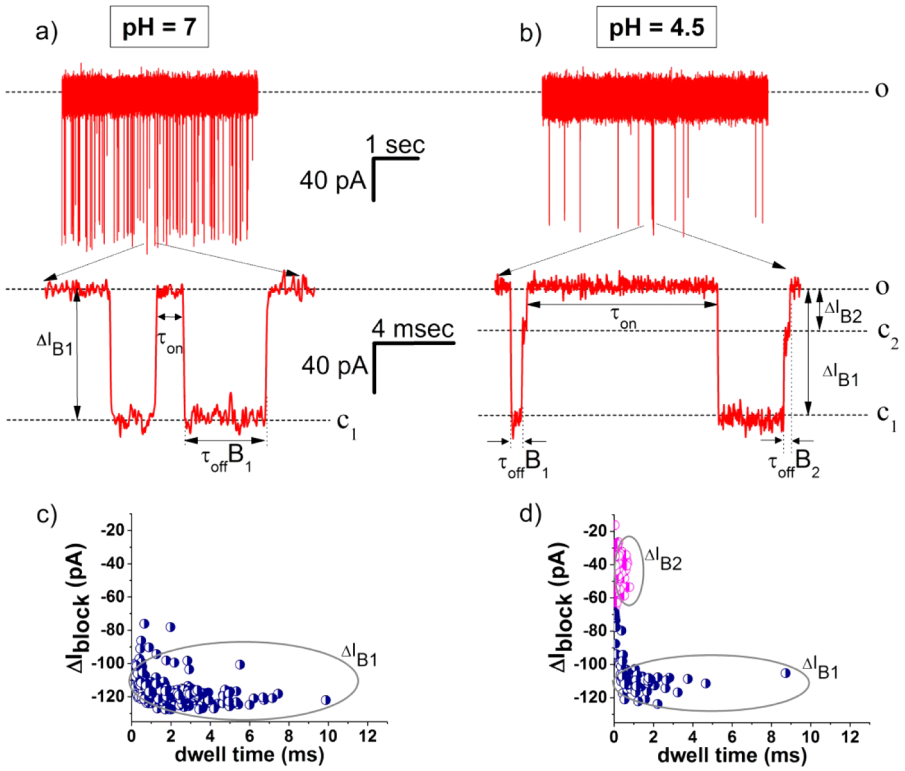

Figure 1. Selected current recordings reflecting the CAMA 3 peptide interaction with the α-HL pore embedded in a lipid membrane. The applied transmembrane potential was ΔV = +70 mV, and experiments were performed in symmetrical added buffer containing 2 M KCl at pH = 7 (panel a) and pH = 4.5 (panel b), with 30 μM peptide applied to the trans side of the membrane. Dotted lines in panels a and b marked by "O" show the level of open-pore current through the α-HL, whereas downward spikes to substates denoted by C_1 and C_2 (see also text) reflect reversible reduction of pore current induced by the interaction of a single peptide with the α-HL. The zoomed-in trace segments under panels a and b reveal the distinct blockage substates, B_1 and B_2, characterized by relative amplitudes denoted by ΔI_{B1} and ΔI_{B2}, associated with a single peptide residing either in the protein's β-barrel or its vestibule during its passage through the pore at various pH values, and display examples of time intervals measured in between peptide–α-HL blockage events (τ_{on}), as well as durations of dissociation times of a single peptide from the β-barrel ($\tau_{off}B_1$) and protein's vestibule, respectively ($\tau_{off}B_2$) (see also text). The distinct B_1 and B_2 blockage substates are visualized in panels c and d, which are scatterplots of dwell time vs relative blockage amplitude of blockage events. The B_1 state at pH = 7 (panel c) and the B_2 state at pH = 4.5 (panel d) are also shown.

water. To suppress electromagnetic and mechanic interference, the bilayer chamber was enclosed in a Faraday cage (Warner Instruments, USA), and placed on the top of a vibration-free platform (BenchMate 2210, Warner Instruments, USA). All experiments were carried out at room temperature of ~23 °C. Electric currents mediated by a single α-HL protein pore immobilized in a lipid membrane, in the absence or presence of peptides, were detected and amplified via a Multi Clamp 700B amplifier (Molecular Devices, USA) set to the voltage-clamp mode, and filtered at 30 kHz with the built-in low-pass Bessel filter. Data acquisition was performed with a NI 6251 acquisition board (National Instruments, USA) at a sampling frequency of 80 kHz, with customized routines written in the LabVIEW 8.20 (National Instruments, USA). When the experiments were carried out under salt gradients, the transmembrane potential bias across the α-HL stemming from its slight anionic selectivity was offset by the voltage compensation knob on the amplifier, prior to applying the voltage (ΔV) across the membrane. The statistical analysis on the relative blockage amplitudes induced by peptides on the electric current through a single α-HL protein, as well as the frequency and duration of the peptides-induced current blockades were analyzed within the statistics of exponentially distributed events, as previously described,[19,55] whereby the average time values separating two consecutive blockage events (τ_{on}) and average blockage time (τ_{off}) were employed to derive association ($rate_{on}$) and dissociation ($rate_{off}$) reaction rates describing the reversible interaction between peptides and the α-HL protein. Data graphing and statistics were mainly done with the help of the Origin6 (Origin Lab, USA) and pClamp 6.03 (Axon Instruments, USA) software. At least three independent experiments were carried out in order to arrive at the numerical estimates reported herein. In all the analyses, we excluded the distinct population of very fast occurring, low-amplitude spikes, which reflected blockage events due to peptide bumping into the pore mouth, and not the actual capture events of the peptide into the inner region of the α-HL β-barrel.

RESULTS AND DISCUSSION

1. Interaction between Histidine-Containing, β-Hairpin-like Peptides and the α-HL Pore at Neutral and Acidic pH. The insertion of a single α-HL protein pore into a stable lipid membrane bathed in a buffered solution containing 2 M KCl at pH = 7, resulted in an "open-pore" current of 125.6 ± 1.5 pA (denoted by "O"), measured at an applied holding potential of ΔV = +70 mV. The trans side addition of 30 μM of the CAMA 3 peptide gave rise to reversible blockages of the α-HL open-pore current, seen as downwardly pointing spikes (Figure 1, panel a). Such events were associated with individual peptide passages from the bulk, trans side buffer to the protein β-barrel, where it temporarily blocked the ionic current through steric occlusions, before its transport to the cis side under the influence of the positive potential difference clamped across the pore. As we noted in previous work,[55] around neutral pH values, the current signature of such peptides–α-HL β-barrel interactions, is characterized by blockage events (C_1) with a homogeneous relative amplitude denoted by $\Delta I_{B1} = I_{C1} - I_O$, where I_O represents the current measured through the free α-

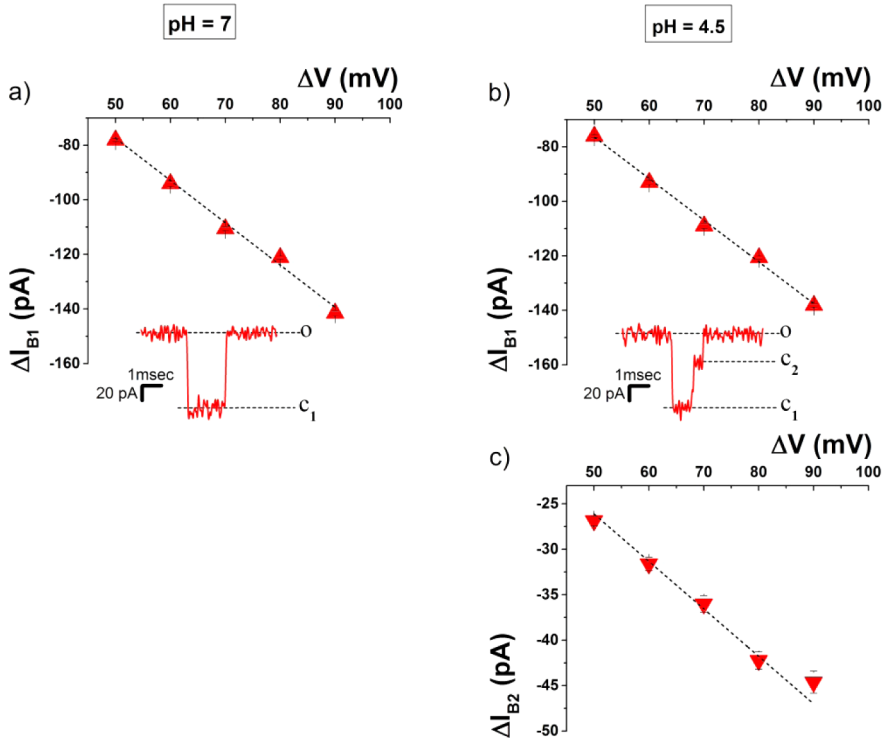

Figure 2. $I-\Delta V$ dependence of the relative blockage amplitudes of events associated with the CAMA 3 peptide–α-HL interactions, corresponding to the C_1 (ΔI_{B1}) and the C_2 substate (ΔI_{B2}), estimated in 2 M KCl, at pH = 7 (panel a) and pH = 4.5 (panel b and c) (see also Figure 1), with the corresponding linear fit through "zero" (dotted lines). The insets in panels a and b show selected CAMA 3 peptide-α-HL blockage events, facilitating the view on the distinct C_1 and C_2 blockage substates (see also text).

HL pore, and I_{C1} the residual current measured through the pore while a single peptide resides in its β-barrel.

At pH = 4.5, chosen in the present study to facilitate the histidine residues protonation (pK_a histidine ~6.5), the recorded current traces revealed the emergence of a second blockage substate, denoted C_2, characterized by a smaller relative magnitude ($\Delta I_{B2} = I_{C2} - I_O$, where I_{C2} represents the residual current through the α-HL protein while a single peptide resides in its vestibule) (Figure 1, panel b). We reported on this observation extensively in recent work performed with structurally related peptide constructs,[55] and concluded that among others, the enhanced anion-selectivity of the wild type α-HL manifested at acidic pH values, augments the electro-osmotic, cis-to-trans flow of water through the protein pore, serving as a "hydrodynamic molecular brake" able to slow down the trans-to-cis electrophoretic-driven motion of the peptide, down the potential gradient. Due to the size difference between α-HL's β-barrel (inner diameter of ~20 Å) and its vestibule (average diameter of ~46 Å), the distinct current blockades are associated with the transient dwelling of the peptide in either α-HL's inner nanocavities (i.e., the inner β-barrel or vestibule region) which, as a result of peptide's slowed down motion along the electric fields within the protein pore, become visible within the time resolution of our recording system. By judging the two distinct transient current blockages in the frame of volume-exclusion arguments, we assigned the higher blockage level of relative blockage amplitude ΔI_{B1} to the peptide residing in the α-HL's β-barrel, and the lower blockage level of relative blockage amplitude ΔI_{B2} to the peptide present inside the α-HL's vestibule.[55]

The main observations stemming from the snapshot traces shown in Figure 1 are (i) the time interval measured in-between CAMA 3 peptide-induced blockage events (τ_{on}) increases with increasing the buffer acidity from pH = 7 to 4.5 (Figure 1, panels a and b); (ii) the dwell times correspondig to the peptide temporary residence within α-HL's β-barrel, assimilated to the B_1 substate ($\tau_{off}B_1$), decrease with decreasing the pH from 7 to 4.5 (Figure 1, panels c and d); (iii) the relative blockage amplitude of the B_1 substate (ΔI_{B1}) gets reduced as the pH changes from pH 7 to 4.5 (Figure 1, panels c and d). All experiments were undertaken multiple times, providing essentially similar results.

As indicated by the scatterplots in Figure 1, panels c and d, and documented before,[55] the passage of the peptide along the α-HL's vestibule at pH = 7, gives rise to blockage events which have dwell times too short, making them undetectable at our system's time resolution, so the statistics on B_2-like events can only be performed at pH = 4.5.

A statistical analysis of each current trace in which we separated bumping and translocation events, allowed us to extract quantitative information regarding the β-barrel and vestibule translocation rates of the CAMA 3 peptide at the applied potential ΔV = +70 mV ($rate_{on}B_{1(pH=7)} = (13.23 \pm 0.92)s^{-1}$, $rate_{on}B_{1(pH=4.5)} = (1.17 \pm 0.08)s^{-1}$, $rate_{off}B_{1(pH=7)} = (520.40 \pm 36.62)\ s^{-1}$, $rate_{off}B_{1(pH=4.5)} = (966.85 \pm 68.27)\ s^{-1}$), and the voltage-dependence of open-pore α-HL current blockages induced by a peptide transiently trapped within the β-barrel region, or its vestibule, in neutral (pH = 7) and acidic (pH = 4.5) buffers (Figure 2).

The residual conductance of the α-HL, temporarily blocked by a single peptide residing in either the β-barrel or vestibule, is approximately constant vs ΔV (Figure 2), meaning that the α-HL-trapped peptide does not deform significantly across voltages imposed during experiments. For the present study,

and as we will show below, the usefuleness of the statistical analysis on such current blockages lies in the possibility of inferring quantitative peptide volumetric information (i.e., peptide size), while it resides in the α-HL's β-barrel and its vestibule, by resorting to the theory of resistive pulse measurements.[61] Within simplifying assumptions, if the protein nanopore is represented as a uniformly sized cylinder of length (l_{pore}) and diameter (d_{pore}), immersed in a buffer of electrical conductivity (σ), and clamped at a potential difference (ΔV), the volume (δ) of a peptide that enters the nanopore and entails a relative current blockage of ΔI ($\Delta I = I_{blocked} - I_{open}$, where I_{open} denotes the open-pore current in the absence of the peptide and $I_{blocked}$ the residual current across the pore with a peptide in it) can be written as the following:

$$\delta = \frac{\Delta I(l_{pore} + 0.8d_{pore})^2}{\gamma\sigma\Delta V} \quad (1)$$

In eq 1, γ is a unitless shape parameter that equals 1.5 or 1.0, depending on whether the nanopore-residing peptide is modeled either as a globular sphere or long cylinder aligned parallel to the electric field within the nanopore, and the peptide's length ($l_{peptide}$) is assumed to be smaller than the effective length of the pore (l_{eff}), where $l_{eff} = (l_{pore} + 0.8d_{pore})$.[62]

As demonstrated previously for structurally related peptides,[43,48,50] supplementary analysis revealed that both association ($rate_{on}$) and dissociation ($rate_{off}$) rates increase with an increase in the electric force action on peptides (data not shown). Within a simplified model in which the interactions between the peptides and the α-HL can be described as a chemical reaction, this can be qualitatively understood within the classical transition state relation, whereby the positively charged peptides capture on the trans side of the membrane (or its subsequent release from the pore), involves overcoming a free energy barrier (ΔG^*) that is lowered by the trans positive applied potential (ΔV) with the δG value, thus increasing the corresponding association (or dissociation) reaction rate constant (k) to and from the β-barrel ($k = (k_B T/h)\kappa e^{-((\Delta G^* - \delta G)/k_B T)}$); k_B represents the Boltzmann's constant, T the absolute temperature, h the Planck's constant, and κ the transmission coefficient).[42]

To account for why the CAMA 3 association rate ($rate_{on}$) decreases with lowering the pH (vide supra for numbers, and Figure 1, panels a and b), one has to consider both enthalpic and entropic changes brought about by the buffer's pH on the free energy barrier, which determines the value of the peptide−α-HL reaction rate of association. The enthalpic contribution can be easily grasped by recalling that at the trans end of the β-barrel, an incoming, positively charged CAMA 3 peptide faces a charged, 7-fold symmetric ring, composed of 14 aspartic acids (Asp 127 and Asp 128) and 7 lysines (Lys 131) from the 7 α-HL monomers, which, at pH = 4.5, assumes a lesser negative charge as compared to that at neutral pH.[63] Therefore, the mouth of the α-HL's β-barrel behaves as an electrostatic barrier for the incoming positively charged peptides, causing the lowering of the local peptides concentration near the β-barrel trans entrance. In addition, at pH = 4.5, the protonation of the peptide's histidine residues leads to an augmentation of the inter-residues electrostatic repulsion interactions as compared to those manifested under neutral conditions (pH = 7), which leads to the prevalence of a more spatially disordered peptide at the trans side mouth of the β-barrel. Knowing that the probability of successful threading into the pore is determined by the internal dynamics of the peptide,[63,64] we propose that at acidic pH = 4.5, the peptide is likely to spend a larger amount of time in search for an entropically favorable conformation before a successful translocation through the confined topology of the β-barrel occurs.

Further to this, from experiments performed at pH = 4.5, we noted that the amplitude of the current blockage generated by a CAMA 3 peptide residing in the α-HL's β-barrel ($\Delta I\ B_1$) was smaller than the value seen at neutral pH (Figure 2, panels a and b). In a minimalist model, by neglecting surface charge-mediated, ion current contributions, which might add to the net electric flow through the protein while a peptide resides within the pore,[65,66] and by invoking eq 1, data shown in Figure 2 constitute a good indication that histidines protonation induces a partially structured intermediate which behaves as a less-stable hairpin at acidic pH values, thus obstructing to a lesser extent the protein pore. This is in agreement with our previous data, demonstrating that larger cross section areas are available for the current through the α-HL upon passing an unfolded single stranded peptide vs a kinked hairpin.[55] It should be mentioned that in support to this interpretation, previous work established that interactions between charged residues contribute to peptide stability, and acidic pH destabilizes folded, small helical proteins, which reach complete unfolding at pH 3.0 mainly due to the protonation of histidines.[67,68]

Another relevant observation is the dissociation rate of the CAMA 3 peptide from the α-HL's β-barrel ($rate_{off}B_1$) is higher at pH = 4.5 as compared to that measured at neutral pH (Figure 1 and estimated values, vide supra), and one reason for this is the increase in electrophoretic force acting on the peptide, as a result of the net gain in positive charge of the peptide caused by the histidines protonation. In addition, and by resorting to the data presented above, we interpreted this as being partly a consequence of the fact that acidic pH-triggered conformational changes of the CAMA 3 peptide from a folded, kinked hairpin, to a partially extended conformation having a smaller average cross-sectional area (vide supra), lead to an increase in the peptide mechanical mobility within the pore, seen through faster translocation times across the β-barrel. This interpretation is in agreement with previous work, showing that for β-hairpin peptides, the translocation through the α-HL protein is faster when the peptides assume an extended conformation.[46]

Nevertheless, a distinct contribution to the peptide passage kinetics across the pore and possibly modulation of its folding substates may arise from the electrostatic interactions with the inner walls of the α-HL protein. In previous work,[63] authors established that at neutral pH values, the β-barrel entrance of the α-HL is negatively charged, whereas the constriction and vestibule regions are largely neutral, while in the vicinity of pH = 4.5, the net charge on the β-barrel entrance is less negative, and the constriction and the vestibule regions become positively charged. Thus, due to the heterogeneity in charge distribution inside the protein at various pH values, one cannot exclude a priori the possible involvement of long-range electrostatic interactions between the CAMA 3 peptide and the α-HL's inner surface, which may influence distinctly the α-HL-confined, peptide behavior. However, such electrostatic interactions are likely to manifest mostly at lower salt concentrations, because around 2 M KCl, the Debye length is $\kappa^{-1} \approx 1.9$ Å, which is a low value relative to the average diameter of the β-barrel (≈20 Å) and vestibule (≈46 Å).

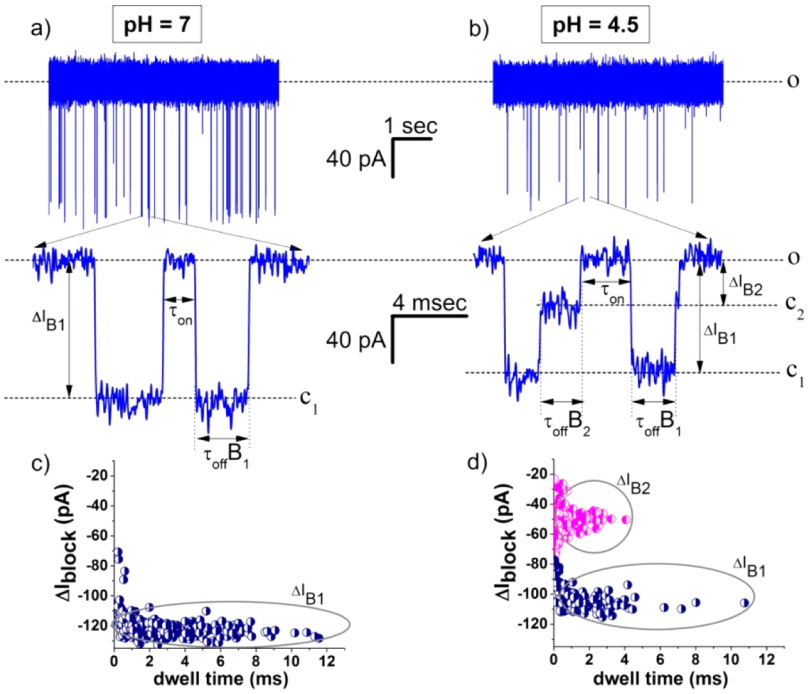

Figure 3. Selected original traces showing the CAMA 1 peptide interaction with the α-HL pore at an applied transmembrane potential of ΔV = +70 mV, in symmetrical buffers containing 2 M KCl at pH = 7 (panel a) and pH = 4.5 (panel b), with 30 μM peptide applied to the trans side of the membrane. The level of open-pore current through the α-HL (dashed lines in panels a and b) is marked by "O", and stochastic events representing reduction of pore current induced by the interaction with a single peptide to substates denoted by C_1 and C_2 are shown (downward spikes). As in Figure 1, the zoomed-in, traces excerpts below panels a and b display, at increased time resolution, distinct blockage substates, whose relative amplitudes are denoted by ΔI_{B1} and ΔI_{B2}, and are associated with a single peptide residing either in the β-barrel or protein's vestibule during its passage through the α-HL, at various pH values. Representative time intervals measured in between peptide–α-HL blockage events (τ_{on}), as well as durations of dissociation times of a single peptide from the β-barrel ($\tau_{off}B_1$) and protein's vestibule ($\tau_{off}B_2$) are shown. Scatterplots shown in panels c and d display the dwell time vs relative blockage amplitude of blockage events associated with B_1 and B_2 blockage substates at pH = 7 and pH = 4.5.

To facilitate a proof-of-concept evaluation of the roles played by histidines in the pH-tuned folding of such model β-hairpin-like peptides, we devised experiments with an additional peptide construct termed CAMA 1, engineered on the CAMA 3 scaffold, with similar charge at neutral pH, hydrophobicity, and size as CAMA 3 (Table 1), but containing only a single histidine residue.

As a first observation, we find that in neutral buffers (pH = 7) and at an applied transmembrane potential ΔV = +70 mV, the association rate of the CAMA 1 peptide to the α-HL protein (rate_{on}) is ~2 times smaller than that of the CAMA 3 peptide, under similar working conditions (see Figure 3 and numbers below). To explain this, we propose that despite having a similar net charge, the presence of an extra histidine favors the prevalence of nonelectrostatic, histidine-mediated inter-residues interactions on CAMA 3 as compared to CAMA 1 peptide, that diminish the conformational entropy of the peptide chain, thus lowering the number of CAMA 3 peptide unsuccessful attempts to entering the α-HL's β-barrel, and therefore decreasing the free energy barrier for the CAMA 3–α-HL association.[63] Under simplifying assumptions, whereby due to their similar size and charge at pH = 7, the standard state, molar enthalpy variation associated with the formation of the peptide–pore transition state during the association reaction (ΔH^*) is identical for both CAMA 3 and CAMA 1 peptides, we estimated the difference of the variation in standard state molar entropies ($\Delta\Delta S^*$) associated with the formation of the CAMA 3– and CAMA 1–α-HL transition state. To proceed, we worked within a simplified model in which the interactions between the peptides and the α-HL's β-barrel can be described as a chemical reaction, characterized by the association rate constant $k_{on} = (k_B T/h)\kappa e^{-((\Delta G*)/RT)}$, where R is the gas constant, and the meanings of other terms are as explained previously, and ΔG^* reflects the standard state, molar free energy variation associated with the formation of the peptide–pore transition state during the association reaction. Knowing that the association reaction rate (rate_{on}) of both CAMA 3 and CAMA 1 peptides equals $\text{rate}_{on} = [\text{peptide}]k_{on}$, one can write

$$\frac{\text{rate}_{on;\text{CAMA 3}}}{\text{rate}_{on;\text{CAMA 1}}} = \frac{k_{on;\text{CAMA 3}}[\text{CAMA 3}]}{k_{on;\text{CAMA 1}}[\text{CAMA 1}]} = \frac{\frac{k_B T}{h}\kappa e^{-\left(\frac{\Delta G^*_{\text{CAMA 3}}}{RT}\right)}[\text{CAMA 3}]}{\frac{k_B T}{h}\kappa e^{-\left(\frac{\Delta G^*_{\text{CAMA 1}}}{RT}\right)}[\text{CAMA 1}]} \quad (2)$$

where $\Delta G^*_{\text{CAMA 3}}$ and $\Delta G^*_{\text{CAMA 1}}$ represent the standard state, molar free energy variation associated with the formation of the "CAMA 3-pore" and "CAMA 1-pore" transition state intermediates during the association reaction, and the bulk concentrations of peptides are denoted by [CAMA 3] and [CAMA 1].

By expressing free energy changes in terms of free enthalpy (ΔH^*) and free entropy (ΔS^*) changes for both peptide, and knowing that the concentration of peptides ([peptide]) was kept similar, eq 2 becomes

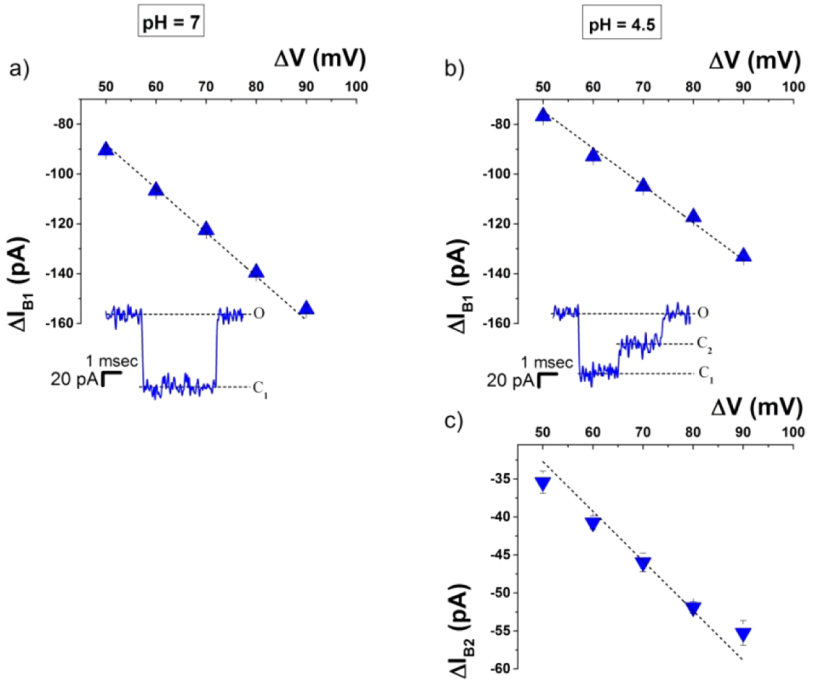

Figure 4. $I-\Delta V$ dependence of the relative blockage amplitudes induced by the CAMA 1 peptide on a single α-HL protein, associated with the C_1 (ΔI_{B1}) and the C_2 substate (ΔI_{B2}) (see Figure 3), estimated in 2 M KCl, at pH = 7 (panel a) and pH = 4.5 (panels b and c), with the corresponding linear fit through "zero" (dotted lines). The insets in panels a and b show selected CAMA 1 peptide–α-HL blockage events, facilitating the view on the distinct C_1 and C_2 blockage substates.

$$\frac{\text{rate}_{\text{on;CAMA 3}}}{\text{rate}_{\text{on;CAMA 1}}} = \frac{e^{-\left(\frac{\Delta H^{*}_{\text{CAMA 3}} - T\Delta S^{*}_{\text{CAMA 3}}}{RT}\right)}}{e^{-\left(\frac{\Delta H^{*}_{\text{CAMA 1}} - T\Delta S^{*}_{\text{CAMA 1}}}{RT}\right)}} = e^{\left(\Delta S^{*}_{\text{CAMA 3}} - \Delta S^{*}_{\text{CAMA 1}}/R\right)} = e^{\left(\Delta\Delta S^{*}_{\text{CAMA 3–CAMA 1}}/R\right)} \quad (3)$$

where by $\Delta\Delta S^{*}_{\text{CAMA 3–CAMA 1}} = \Delta S^{*}_{\text{CAMA 3}} - \Delta S^{*}_{\text{CAMA 1}}$, we denote the difference of the variation in standard state molar entropies (ΔS^{*}) associated with the formation of the 'CAMA 3-pore' and 'CAMA 1-pore' transition state intermediates. Simple algebra reveals that $\Delta\Delta S^{*}_{\text{CAMA 3–CAMA 1}} = R\ln\left(\frac{\text{rate}_{\text{on;CAMA 3}}}{\text{rate}_{\text{on;CAMA 1}}}\right) = 4.7$ J K^{-1} M^{-1}. To this end, we highlight the unique capability of the presented approach to provide quantitative insights into the entropic barrier differences of otherwise rather similar peptides to partitioning within confined nanovolumes, which can be used to probe shifts in the relative populations of distinct folding states of peptides that occur in response to precise altering of inter-residue electrostatic, coordinative, or aromatic interactions, via single-point mutagenesis. In the long run, this approach may prove unique in describing peptides and proteins in terms of conformational ensembles, rather than static conformations,[69] especially relevant for a more accurate thermodynamic quantification of the folding/unfolding processes.

Data shown in Figure 3 demonstrate that similar to the case of the CAMA 3 peptide, the time intervals in-between CAMA 1 peptide-induced blockage events on the open-pore current through a single α-HL protein (τ_{on}) increase substantially with lowering the pH from 7 to 4.5, whereas the opposite is seen on the translocation times of CAMA 1 across the α-HL's β-barrel ($\tau_{off}B_1$). In terms of reaction rates, we found: $\text{rate}_{on}B_{1(pH=7)} = 7.5 \pm 0.66$ s^{-1}, $\text{rate}_{on}B_{1(pH=4.5)} = 1.43 \pm 0.13$ s^{-1}, $\text{rate}_{off}B_{1(pH=7)} = 296.45 \pm 24.3$ s^{-1}, $\text{rate}_{off}B_{1(pH=4.5)} = 471.36 \pm 40.36$ s^{-1}. Supplementary, our analysis revealed that the extent of current blockage through the α-HL protein by a β-barrel residing CAMA 1 peptide is smaller at pH = 4.5 than at pH = 7 (Figure 4).

A plausible explanation for these observations is similar to that offered for the case of the data obtained with the CAMA 3 peptide (vide supra), and constructed on: (i) low pH-mediated enthalpic and entropic contributions to an increase in the free energy barrier height for the CAMA 1 peptide-α-HL association reaction and (ii) acidic pH-triggered conformational changes of the CAMA 1 peptide to more extended conformations, with a smaller average cross-sectional areas, and increased mechanical mobility within the pore.

Remarkably though, at neutral pH, the reaction rate associated with the translocation of CAMA 1 peptides across the α-HL's β-barrel ($\text{rate}_{off}B_{1(pH=7)} = 296.45 \pm 24.3$ s^{-1}) is smaller than that measured for the CAMA 3 peptide ($\text{rate}_{off}B_{1(pH=7)} = 520.40 \pm 36.62$ s^{-1}) (see also original data shown in Figures 1 and 3). This is unexpected because both peptides carry an identical charge at pH = 7, and while their electrostatic energy within the potential gradient inside the α-HL pore is similar, this should lead to largely similar dissociation rates from the pore. Equally interesting is the observation that under same neutral pH conditions, the extent of current blockage induced by a β-barrel residing peptide is slightly larger for the CAMA 1 than CAMA 3 peptide (see data presented in Figure 4 and Figure 2). In relation to this, the volumetric evaluation made based on eq 1 revealed that at an applied transmembrane potential of $\Delta V = +70$ mV and pH = 7, the volume ratio of CAMA 1 and CAMA 3 peptides confined to the β-barrel equals $\delta_{\text{CAMA 1}}/\delta_{\text{CAMA 3}} = 1.11$.

These experimental observations lead us to propose that the particular folding substate of the CAMA 1 peptide endowed by the existence of only one histidine, favors a spatial

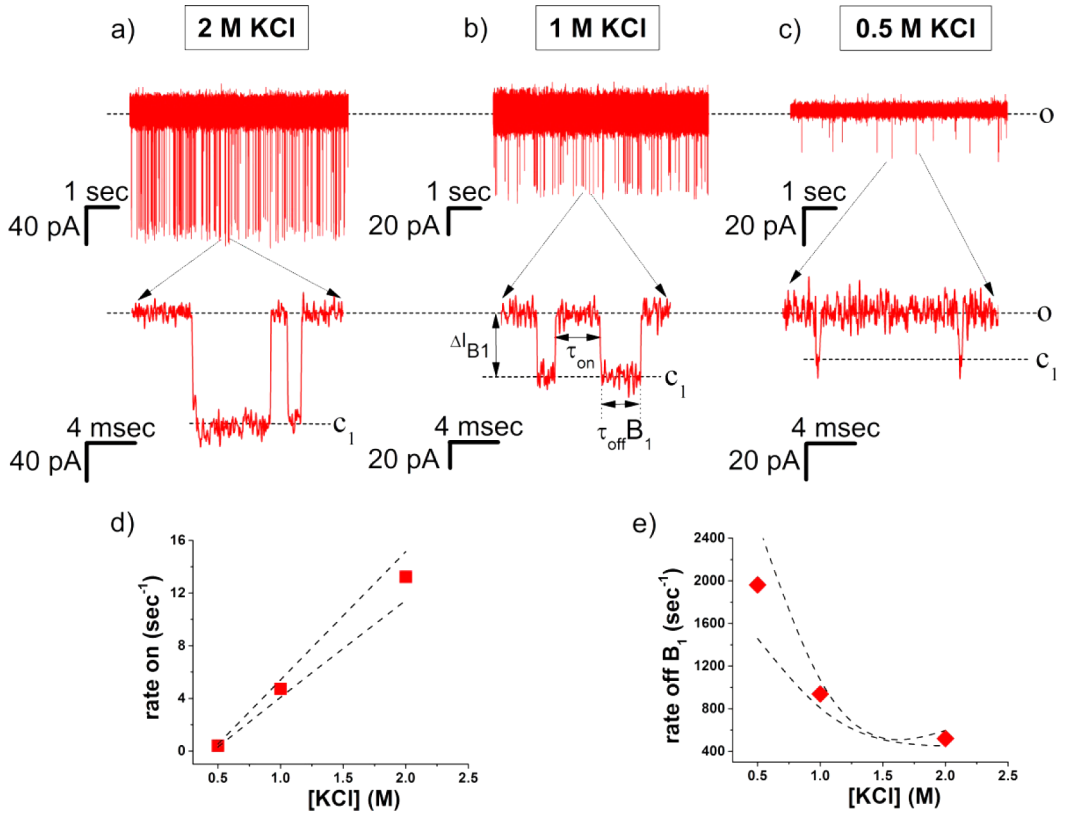

Figure 5. Representative traces demonstrating the salt-dependence of CAMA 3–α-HL interactions. All experiments were carried out at pH = 7, with the peptide added on the trans chamber at a concentration of 30 μM, an applied transmembrane potential of ΔV = +70 mV, and KCl was added symmetrically on both cis and trans chambers at concentrations of 2 M (panel a), 1 M (panel b), and 0.5 M (panel c). The zoomed-in trace segments shown below reveal the distinct blockage substate C_1 characterized by the relative amplitude ΔI_{B1} assigned to the presence of a single peptide within the α-HL's β-barrel at various salt concentrations, and pinpoint examples of time intervals in between peptide–α-HL blockage events (τ_{on}), as well as durations of dissociation times of a single peptide from the β-barrel ($\tau_{off}B_1$). In panels d and e, we represent the outcome of the statistical analysis on such traces, showing the salt dependence of the association ($rate_{on}$) and dissociation ($rate_{off}$) rates characterizing the reversible peptide–α-HL interactions, and the dashed lines represent the 95% confidence domain for these estimated values.

conformation of it inside the α-HL pore distinct from that of the CAMA 3 peptide, which facilitates more prominent interactions of CAMA 1 with the inner walls of the pore, increases its friction, reduces its mobility within the pore, and obstructs the ionic flow across the α-HL pore to a larger extent than the CAMA 3 peptide. Obvioulsy, more elaborate mutagenesis experiments coupled with molecular dynamics simulations of the peptide/nanopore microsystem are needed to clarify the influence of the number of histidine residues and their position in the primary structure, on the folding pathways of such peptides. To this end though, our data indicate that it is possible to use the α-HL pore to discriminate among various types of peptides, with similar mass and charge, based solely on their folding behavior.

At pH = 4.5, dissociation rates of the CAMA 1 peptide from both the β-barrel ($rate_{off}B_1$ = 471.36 ± 40.36) and vestibule ($rate_{off}B_2$ = 388.53 ± 37) are smaller than those measured for the slightly higher positively charged CAMA 3 peptide, under similar experimental conditions ($rate_{off}B_1$ = 966.85 ± 68.27 s^{-1}, $rate_{off}B_2$ = 1928.02 ± 184.47 s^{-1}) (see also original data shown in Figures 1 and 3). At least in part, this can be explained by an increase in the electrophoretic transport force acting on the CAMA 3 peptide at acidic pH. Similar to the case of the CAMA 3 peptide, we noted that the relative blockage amplitude of the β-barrel induced by the CAMA 1 peptide (ΔI_{B1}) is smaller at pH = 4.5, as compared to pH = 7 (Figure 4, panels a and b). This can be understood through similar arguments as presented above, i.e. the acidic pH-mediated potentiation of unfolding of the hairpin-like conformation of the CAMA 1 peptide, which therefore tends to obstruct to a lesser extent ions migration across the α-HL pore in acidic buffers.

More interesting is the fact that while residing in the α-HL's vestibule, the relative current blockage (ΔI_{B2}) induced by the CAMA 1 peptide, measured at pH = 4.5, is slightly larger than that of the CAMA 3 peptide (see data shown in Figure 2, panel c and Figure 4, panel c). By using eq 1, the volume ratio of the CAMA 1 and CAMA 3 peptides inside the protein vestibule at pH = 4.5 was calculated ($\delta_{CAMA\ 1}/\delta_{CAMA\ 3}$ = 1.276). We propose that in acidic buffers, the CAMA 1 peptide assumes a more folded spatial structure as compared to that of CAMA 3, allowing it to block, to a larger extent, the current through the protein as compared to the CAMA 3 peptide. In part, this is caused by the augmented electrostatic inter-residues interactions on the CAMA 3 peptide, which has an extra-protonated histidine, allowing for a more extended conformation of it inside the α-HL, as compared to the CAMA 1 peptide. As we will present below, we arrived at a similar conclusion when working at various ionic strengths, strengthening the idea that augmented inter-residues electrostatic interactions manifested at lower salt concentrations play an important role in distorting the hairpin-like structure of the studied peptides. These facts constitute a compelling indication supporting the paradigm

dx.doi.org/10.1021/am5031177 | ACS Appl. Mater. Interfaces 2014, 6, 13242–13256

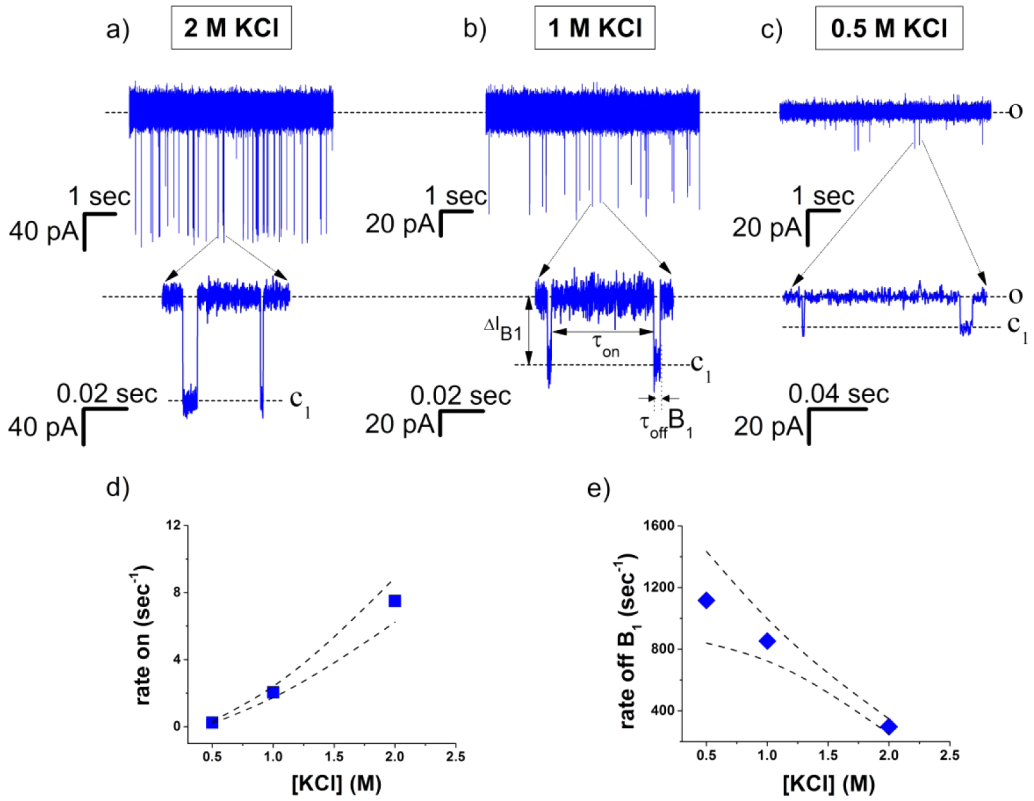

Figure 6. Representative traces revealing the salt-dependence of CAMA 1−α-HL interactions. As for data shown in Figure 5, experiments were carried out at pH = 7, with CAMA 1 added on the trans chamber at a concentration of 30 μM, an applied transmembrane potential of ΔV = +70 mV, and KCl was present in both cis and trans chambers at concentrations of 2 M (panel a), 1 M (panel b), and 0.5 M (panel c). The zoomed-in trace segments shown below reveal the distinct blockage substate C_1 of relative amplitude ΔI_{B1} associated with the presence of a single peptide within the α-HL's β-barrel at various salt concentrations, and display examples of time intervals in between peptide-α-HL blockage events (τ_{on}), as well as durations of dissociation times of a single peptide from the β-barrel ($\tau_{off}B_1$). In panels d and e, we show the result of the statistical analysis on such traces, demonstrating the salt dependence of the association ($rate_{on}$) and dissociation ($rate_{off}$) rates characterizing the reversible CAMA 1 peptide−α-HL interactions, and the dashed lines represent the 95% confidence domain for these estimated values.

according to which the pH-triggered transitions of such peptides from a hairpin-like conformation seen at neutral pH, to partial unfolded topologies encountered at acidic pH values, are prevalent for peptides with more protonable, histidine-residues, and this can be accounted for in simplest terms from an electrostatic perspective (vide supra). We stress that although appealing, this is an oversimplified view of the problem, given that in relation to inter-residues interactions, histidines are amenable to other than electrostatic interactions types, (e.g., cation−π, π−π stacking, hydrogen−π, and hydrogen bond interactions).[58]

2. Interaction between Histidine-Containing, β-Hairpin-like Peptides and the α-HL Pore at Various Ionic Strenghts, at Neutral and Acidic pH. To examine further the influence of electrostatic interactions on the conformational folding of the studied peptides, we carried out experiments at distinct salt concentrations, buffered at pH = 7 and 4.5. Typical current recordings obtained for interaction between the α-HL pore and CAMA 3 peptide at three different KCl concentrations, i.e., 2, 1, and 0.5 M, and pH = 7, are displayed in Figure 5.

As all graphs in Figure 5 are rendered on a similar time axis, the first notable observation is that the peptide association times (τ_{on}) increase with lowering the ionic strength in the buffer, while the opposite occurs for the pore's blockage duration be a single peptide (τ_{off}). The statistical analysis yielded values of association ($rate_{on}$) and dissociation reaction rates ($rate_{off}$) characterizing the dynamics of CAMA 3−α-HL interactions at varying salt concentrations (Figure 5, panels d and e).

Recalling that the magnitude of the electrostatic interactions manifested between the negatively charged entrance of the α-HL's β-barrel and the positively charged peptides, are among crucial factors determining the peptide−protein pore association rate (vide supra), the first relevant observation, namely that the peptide capture ($rate_{on}$) gets considerably diminished as ionic strength decreases, is unexpected and counterintuitive. That is, one would expect that a decrease in the KCl concentration that entails an augmentation in the magnitude of attractive electrostatic interactions between the peptide and the protein pore, due to the increase in the Debye length (κ^{-1} $\approx$ 1.9 Å at 2 M KCl; κ^{-1} $\approx$ 3 Å at 1 M KCl; κ^{-1} $\approx$ 4 Å at 0.5 M KCl), results in the net increase of the peptide capture rate, via a decrease in the free energy barrier of peptide association to the pore, through enthalpy-related effects.[63] In addition, the above-mentioned potentiation of attractive electrostatic interactions between the peptides and the protein pore manifested in low salt buffers increases the local concentration of peptides near the trans mouth of the α-HL's β-barrel, which would reflect in a proportional increase of the peptide association rate to the α-HL pore. One should note that regardless of the salt concentration added symmetrically in the cis and trans chambers, at a fixed transmembrane potential value set from an external source (ΔV), the net potential difference across the

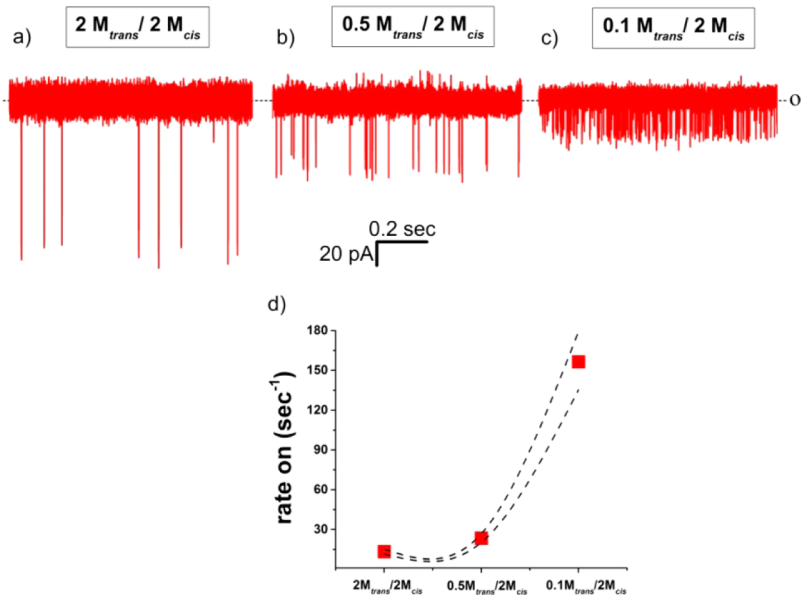

Figure 7. Representative electrophysiology traces demonstrating the augmenting effect of the salt concentration gradient upon the trans-added CAMA 3 peptide capture by the α-HL pore, at neutral pH. The peptide concentration was 30 μM throughout. The trace shown in panel a was obtained by recording the peptide–α-HL interactions with KCl added symmetrically at a 2 M concentration in both chambers, whereas traces shown in panels b and c are representative for the peptide–α-HL interactions when the KCl concentration in the cis chamber was kept at 2 M, and that on the peptide addition chamber (trans) was set to 0.5 and 0.1 M, respectively. The transmembrane potential was similar throughout, ΔV = +70 mV. The individual points shown in panel d display the quantitative evaluation of the peptide capture rate (rate on) vs the salt gradient, and the dashed lines represent the 95% confidence domain for these estimated values.

trans and cis chambers, as well as the protein pore, remains invariant (see the Supporting Information, '*Electric circuit analysis of a voltage-clamped nanopore, exposed to a salt gradient*'), meaning that the electrophoretic force acting of the incoming peptides from the trans chamber is similar at all salt concentrations.

A plausible explanation for the peptide capture rate reduction in low salt concentration buffers relies on the fact that the increased value of the Debye length in low ionic strength buffers entails an increase in the radius of counterions cloud around the peptide, which hinders a peptide's subsequent partition into the narrow β-barrel of the α-HL pore. This is in good agreement with previous work in which the capture and transport of dextran sulfate molecules through a α-HL protein was shown to diminish as the salt concentration in the buffer decreased.[39] As we discussed above, an additional contribution to the reduction in peptide capture rate in low-salt buffers may stem from a conformational entropy gain of the peptide chain, mediated by augmented inter-residues interactions manifested in low Debye length buffers, which compete with the additional enthalpic contribution to free energy barrier for the CAMA 3–α-HL association, brought about by increased peptide–α-HL electrostatic interactions.

From similar experiments undertaken with the CAMA 1 peptide, summarized by the data shown in Figure 6, we came across a yet another intriguing result, namely despite their similar charge, the extent of low-salt-mediated decrease in the CAMA 3 and CAMA 1 peptide capture rate by the α-HL protein is dissimilar at neutral pH. That is, by lowering the KCl concentration from 2 to 0.5 M, the capture rate of CAMA 3 peptide decreases slightly more in relative terms as compared to that of CAMA 1 peptide, namely $\text{rate}_{\text{on;CAMA 3}}[0.5\text{M}] = 3\% \times (\text{rate}_{\text{on;CAMA 3}}[2\text{M}])$ whereas $\text{rate}_{\text{on;CAMA 1}}[0.5\text{M}] = 3.3\% \times (\text{rate}_{\text{on;CAMA 1}}[2\text{M}])$ (see also Figures 5 and 6, panels d and e). In other words, the free energy barrier of peptide–α-HL association (ΔG^*) increases more in 0.5 M KCl as compared to 2 M KCl for the CAMA 3 vs CAMA 1 peptide. Noting that the enthalpy (ΔH^*), electrostatic component of peptides–α-HL interactions is similar at neutral pH for both types of peptides, regardless of salt concentrations, and considering as a rough approximation that entropies of both CAMA 3 and CAMA 1 peptides are similar in the confined space of the α-HL's β-barrel, we posit a greater susceptibility for the CAMA 3 peptide to gain in bulk entropy in low-salt buffers, as compared to CAMA 1, and the molecular details of this mechanism still await deciphering. This result suggests that with further refinements (e.g., mutagenesis of histidines and other charged residues, temperature-dependence data on peptides–α-HL interactions), the presented approach can be used as a new experimental tool to elucidate and understand how the propensity of peptides folding to get destabilized by electrostatic interactions is correlated with the presence and sequence of particular amino acids.

We further found that in low ionic strength buffers, the increase in the electric force acting on the peptide from the externally applied voltage source, leads to an increase in the peptide capture rate, most likely as a result of peptide's counterions cloud squeezing and forced passage of the peptide from the trans buffer to the protein's β-barrel (Figure S1, Supporting Information). In a different approach aimed at the "electrophoretic catalysis" of peptide capture by the α-HL pore in low ionic strength buffers, we worked under distinct asymmetric salt concentration conditions, in which the salt concentration in the cis chamber was kept at 2 M KCl and that on the trans chamber was set at 2, 0.5, and 0.1 M KCl, respectively. As originally proposed by Wanunu et al. for the capture of dsDNA by solid-state nanopores,[64] the peptide capture rate is expected to increase as the salt concentration in

the trans chamber decreases. Typical ionic current traces measured through α-HL pore under such conditions are shown in Figure 7, revealing that unlike experiments carried out in symmetrical ionic strength conditions (vide supra), by maintaining the KCl concentration in the cis chamber at 2 M, the CAMA 3 peptide capture rate increases as the trans salt concentration starts to decrease. That is, by comparing the data shown Figure 5, panel d, with those represented by Figure 7, panel d, it is clear that the hindering effect of low ionic strength buffer on peptide association to the α-HL pore is overcome by a salt gradient maintained with respect to the cis chamber.

As demonstrated in this work under simplifying assumptions (see the Supporting Information, "Electric circuit analysis of a voltage-clamped nanopore, exposed to a salt gradient") and following a distinct route from that of Wanunu et al.,[64] this result can be explained by the fact that the net potential drop across the trans side of the membrane and implicitly the electrophoretic force acting on the peptide increases as the trans salt concentration decreases, despite the fact that the externally applied transmembrane potential (ΔV) is kept invariant (Figure S3, Supporting Information). This prediction was nicely met by our experimental data, as we noted that when the salt concentration gradient was set at (0.5 M KCl trans//2 M KCl cis), the peptide capture rate ($rate_{on}$) became ~57 times higher than that measured under symmetrical salt concentrations (0.5 M KCl trans//0.5 M KCl cis), at the same holding potential ΔV = +70 mV and peptide concentration (for quantitative comparison, see data shown in Figure 5, panel d, and Figure 7, panel d). That is, despite the fact that in both cases, the Debye length and the radius of counterions cloud around the peptide was similar in the trans side, the extra contribution to the electrophoretic force acting on the peptide, arising from the (0.5 M KCl trans//2 M KCl cis salt concentration gradient (see also the Supporting Information), is able to force further the peptide into the α-HL's β-barrel.

We hypothesized that another facet of the reduced electrostatic screening manifested in low salt concentrations is the augmented electrostatic stretching of the CAMA 3 peptide chain inside the α-HL, due to increased inter-residues electrostatic interactions. Data shown in Figure 5, panel e, supports this hypothesis, as we estimated an increased dissociation rate of the CAMA 3 peptide from the α-HL pore ($rate_{off}B_1$) during experiments undertaken in symmetric, lower salt concentrations, at pH = 7. This may be explained by an increased propensity of the CAMA 3 peptide to assume an unfolded conformation in low ionic strength buffers, and therefore an enhanced mechanical mobility through the pore. This interpretation is further strengthened by the fact that as the salt concentration on both chambers decreases, the relative current blockage induced by the pore-residing peptide ($\Delta I_{B1}/I_O$) lowers ($\Delta I_{B1}/I_O[2M] = 0.91$, $\Delta I_{B1}/I_O[1M] = 0.79$, $\Delta I_{B1}/I_O[0.5M] = 0.81$), as it would be expected for a peptide whose effective cross-sectional area decreases (i.e., becoming a more spatially disordered peptide), leading to a lesser degree of open pore current obstruction.

A similar phenomenon was seen when the dissociation of the CAMA 1 peptide from the α-HL pore was evaluated in symmetrically added, lower salt concentrations buffers, at pH = 7 (see Figure 6, panel e), and the relative current blockage ($\Delta I_{B1}/I_O$) was also seen to decrease when lowering the KCl concentration ($\Delta I_{B1}/I_O[2M] = 0.97$, $\Delta I_{B1}/I_O[1M] = 0.84$, $\Delta I_{B1}/I_O[0.5M] = 0.80$). Supplementary to these data, due to the fact that dissociation rate of the CAMA 3 peptide from the pore is higher than that of the CAMA 1 peptide at all salt concentrations (see Figures 5 and 6), we posit the persistence of a more folded conformation substate in the case of the CAMA 1 peptide as compared to the CAMA 3 peptide, while either peptide transits the α-HL pore.

To gain a yet deeper insight into these findings, we studied the salt-dependence of the CAMA 3 peptide–α-HL interactions at acidic pH, whereby the inter-residues electrostatic interactions are expected increase yet more due to the histidine residues protonation, and as a consequence, the salt-mediated unfolding of the peptide would be more prominent. As we display in Figure S4, panel a (Supporting Information), the likelihood of the CAMA 3 peptide–α-HL pore interactions is reduced considerably by the change in buffer acidity to a value of pH = 4.5 (vide supra as well), but as long as ionic strength is concerned, and unlike the experiments performed in pH-neutral buffers (see Figure 5), when the recording chamber contains 1 M and, respectively, 0.5 M KCl added symmetrically, the peptide association to the α-HL pore is virtually absent.

As we presented above and besides entropic effects contributing to this phenomenon (vide supra), one possible mechanism for the acidic pH-induced decrease in the rate of peptide capture at various ionic strengths lies in the attenuation of pore–peptide attractive interactions, as the negative charge at the mouth of the α-HL's β-barrel lowers in acidic buffers, and this apparently does not compensate for the gain in peptide net charge caused by the histidine-residues protonation (the histidine pK_a = 6.5, and to a first approximation, we neglected its variation with ionic strength). Experiments performed under similar conditions but with the CAMA 1 peptide instead, revealed a similar tendency of a decrease in the peptide capture rate at pH = 4.5 as compared to neutral conditions, and this tendency was also dependent on the value of the KCl concentration (Figure S4, panel b, Supporting Information). Interestingly, capture events of the CAMA 1 peptide by the protein pore were still seen in buffers containing as little as 1 M KCl, conditions in which the CAMA 3 peptide showed virtually no successful entry events into the α-HL pore. Within the electrostatic framework depicted above, this is again highly unexpected, as that the net gain in positive charge at acidic pH is lower for the CAMA 1 than that of the CAMA 3 peptide (Table 1), thus leaving the electrostatic interactions between the CAMA 1 peptide and the α-HL's β-barrel less strong as compared to the CAMA 3 peptide at pH = 4.5. In other words, one would have expected that the pH-lowered peptide capture rate would be prevalent in the case of the CAMA 1 peptide, at all salt concentrations.

Our interpretation is that in acidic buffers, the inter-residues electrostatic interactions are more prominent in their effects on the peptide spatial structure for the case of the more charged CAMA 3 than CAMA 1 peptide, and they are further augmented in low ionic strength buffers due to the lesser screened-out effect induced by counterions present in the buffer. Consequently, the lower salt-mediated peptide disordering degree at an acidic pH is larger for the CAMA 3 peptide, making it less prone to be captured by the α-HL's β-barrel, as compared to the CAMA 1 peptide.

As a supplementary check of the proposed explanation regarding the tuning effect of the ionic strength on peptides–α-HL interactions in acidic buffers, we sought to reverse the phenomenon presented in Figure S4 (Supporting Information), by carrying out experiments in which the KCl concentration in the peptide addition, trans chamber, was brought back to 2 M,

while the KCl concentration in the cis chamber was kept at 0.5 M (Figure S5, panels a and b, Supporting Information). Notably, despite the fact that under a such salt gradient (2 M KCl trans//0.5 M KCl cis), the voltage drop across the trans chamber is lower (~4.3 mV) than that calculated under symmetrical conditions (~8.9 mV) (0.5 M KCl trans//0.5 M KCl cis) (Figure S6, Supporting Information), the elevated concentration of salt in the trans chamber recovers to a certain extent the likelihood of the CAMA 3 and CAMA 1 peptide capture by the pore (compare Figure S4, lower traces, measured at 0.5 M KCl, with traces shown in Figure S5, panels a and b, Supporting Information), and this effect is more prevalent for the CAMA 1 peptide, despite its lower charge than CAMA 3 at pH = 4.5. An inverted salt gradient (0.5 M KCl trans//2 M KCl cis) at pH = 4.5 was found ineffective in restoring either peptide's ability to interact with the α-HL protein (Figure S5, panels c and d, Supporting Information), despite the fact that under such conditions, the calculated potential drop across the trans chamber (~16.5 mV; see Figure S3, Supporting Information) is higher than that estimated under symmetrical conditions (~8.9 mV; 0.5 M KCl trans//0.5 M KCl cis) (Figure S6, Supporting Information). We conclude that in acidic buffers, the additional positive charge on both CAMA 1 and CAMA 3 peptides brought by the histidine protonation facilitates a more prevalent low salt-mediated peptide disordering, which entails an entropic barrier that impedes the subsequent favorable capture of peptides by the α-HL. Unlike the case of neutral buffers, in low ionic strength and low pH buffers, a supplementary increase in the electrophoretic force acting on the peptides on the trans side of the membrane, as it occurs either by raising the overall transmembrane holding potential (data not shown) or working under an asymmetrical 0.5 M trans// 2 M cis gradient, fails to restore the likelihood of peptide interaction with the pore.

CONCLUSIONS

We probed herein the reversible interactions between histidine-containing, β-hairpin-like peptides and the α-HL protein when the histidine residues assume either the protonation or deprotonation state, and distinct salt concentrations, by analyzing the peptides-induced modulations of the ionic current through a membrane-immobilized α-HL protein pore, and interpreted the results in terms of folding changes of peptides.

Concisely, the main findings are as follows: (1) as compared to neutral buffers (pH = 7), acidic ones (pH = 4.5) were shown to dramatically decrease the capture rate by the α-HL of either one or two histidine-containing peptide. To explain this, we considered both enthalpic and entropic contributions brought about by the buffer acidity on the free energy barrier, which controls the peptides–α-HL association reaction rate. The enthalpic contribution can be understood through the fact that at acidic pH values, the trans end of α-HL's β-barrel carries a less negative charge as compared to that estimated in neutral buffers, thus behaving as an electrostatic barrier for the incoming positively charged peptides. The entropic contribution lies in that at pH = 4.5, the protonation of peptide's histidine residues leads to a more spatially disordered peptide at the trans side mouth of the α-HL's β-barrel, which lowers its likelihood for a successful entry into the pore. (2) We found that at pH = 4.5 and 2 M KCl, the amplitude of blockages induced by a β-barrel-residing single peptide, with either one or two histidine residues, is smaller than that measured at neutral pH. We interpreted this as pH-induced changes in the conformation of the peptide, which behaves as a less-stable hairpin at acidic pH values, and consequently obstructs to a lesser extent the ions passage across the protein pore. This is also confirmed by the observation that the dissociation rate of the peptides from the α-HL's β-barrel is higher at acidic as compared to neutral pH values, indicating that contributions from the acidic pH-triggered conformational changes from a folded, hairpin-like topology to an extended conformation with a smaller average cross-sectional area, lead to an increase in the peptide mechanical mobility within the pore, and entail a faster translocation time. (3) The magnitude of peptides inter-residues electrostatic interactions and therefore peptide structure distortion from the hairpin-like structure, manifest more prominently at lower salt concentrations. A first solid observation in support of this is the dramatic decrease in peptide capture rate by the α-HL pore, for both one- and two-histidines-containing peptides, as the KCl concentration in neutral buffers decreased from 2 M, to 1 and 0.5 M, respectively. We posit that the increased value of the Debye length in low ionic strength buffers entails an increase in the radius of counterions cloud around the peptide, which hinders its partition into the narrow β-barrel of the α-HL pore. Supplementary, the reduction in peptide capture rate in low salt concentration buffers may stem from the peptide stabilization deficit, resulting from increased electrostatic repulsions within the peptide in low Debye–Hückel screening conditions, and a consequent conformational entropy gain of the peptide chain. (4) In low salt concentrations and neutral pH, an augmented stretching of the one- and two-histidine-containing peptides inside the confined volume of the α-HL occurs, mainly due to increased inter-residues electrostatic interactions. This is supported by two experimental results: (i) the increased dissociation rate of either type of peptide from the α-HL pore with the decrease in the ionic strength, which was correlated to an enhanced mechanical mobility caused by peptides partial unfolding. Notably, the dissociation rate of the two-histidine-containing peptide from the pore is higher than that of the one-histidine-containing peptide at all salt concentrations, which indicate the persistence of a more unfolded conformation substate in the case of the former peptide as compared to the latter one while either peptides transits the α-HL pore, and (ii) as the salt concentration decreases, the relative current blockage induced by the pore-residing peptide also decreases, explained through a low-salt-mediated, stretched-out peptide, and therefore decrease in its effective cross-sectional area blocking the ion transport through the α-HL pore. (5) The frequency of peptides-α-HL pore interactions was reduced considerably at pH = 4.5, and unlike the experiments made in pH-neutral buffers, at salt concentrations of 1 M and, respectively, 0.5 M KCl, and at pH = 4.5, the two-histidine-containing peptide association events to the α-HL pore were largely absent. We posit that at in acidic buffers and below its pK_a, the histidine's protonation facilitates a more prevalent, low salt-mediated peptide disordering, and increases in the radius of the counterions cloud around the peptide, which impedes the subsequent favorable capture of peptides by the α-HL. The fact that the low salt-induced decrease in peptide capture at pH = 4.5, is more prominent for the construct with two as opposed to that with one histidine residue, can be accounted for from an electrostatic perspective whereby the more charged peptide is likely to undergo larger conformational changes in low-salt buffers, through enhanced inter-residues electrostatic interactions facilitated by the reduced charge screening.

In a condensed view, the novel findings stemming from this work, as stated above, are embodied in the representation below (Figure 8).

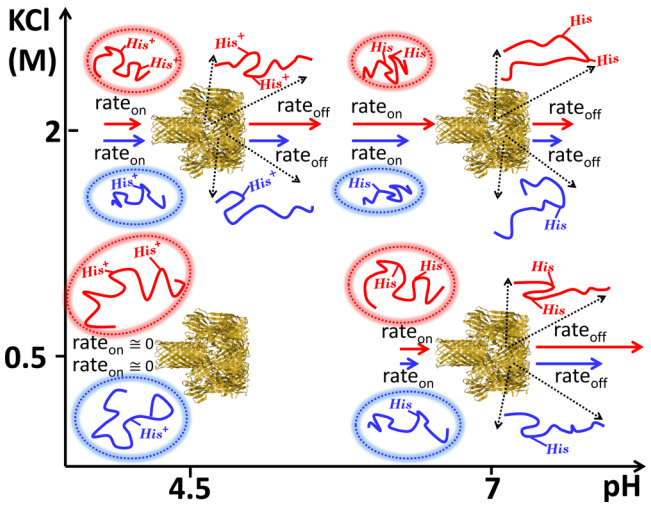

Figure 8. Cartoon representation reflecting the kinetic and folding behavior of the CAMA 3 (two histidine residues) and CAMA 1 (one histidine residue) peptides, at distinct salt concentrations and pH values. Note that peptides and the α-HL protein were not drawn to the scale, and the graphic design of peptides, including the various degree of stretch while they are present within the α-HL pore, were intended to solely capture qualitatively the data presented above. The oval shapes around peptides before interacting with the α-HL, and their corresponding sizes, are a qualitative representation of the counterions clouds around the peptide under the shown experimental conditions. The length of each arrow associated with $rate_{on}$'s and $rate_{off}$'s captures qualitatively, yet in accordance to the experimental data, the proportional changes in the association/dissociation reaction rates characterizing the interactions between distinct peptides and the α-HL's β-barrel, under the shown experimental conditions.

The present work brings supplementary support to the possibility of studying the reversible changes in spatial structure of folded peptides and small proteins of similar mass, through extracting kinetic and single-molecule excluded volumes information from peptides–a-HL pore interactions events. Working in conjunction with nanopore sensors able to achieve temporal resolution of microseconds,[70] this approach may be of unique help in the realm of nanopore-based proteomics technologies, by revealing in real-time rapid changes associated with distinct folding subpopulations of individual peptides of biological significance, as they are induced by chemical and physical factors (e.g., denaturing agents, temperature, salt, pH, etc.), usually invisible in ensemble experiments.

■ ASSOCIATED CONTENT

Supporting Information

Analytical approach toward estimating the electric potential drop across a nanopore immersed in a bathing solution, under asymmetric salt concentrations. This material is available free of charge via the Internet at http://pubs.acs.org.

■ AUTHOR INFORMATION

Corresponding Author

*T. Luchian. E-mail: luchian@uaic.ro.

Author Contributions

The paper was written through contributions of all authors. All authors have given approval to the final version of the paper.

Notes

The authors declare no competing financial interest.

■ ACKNOWLEDGMENTS

The authors acknowledge the financial support offered by grants PN-II-ID-PCCE-2011-2-0027, PN-II-PT-PCCA-2011-3.1-0595, PN-II-PT-PCCA-2011-3.1-0402, and the National Research Foundation of Korea (NRF) grant funded by the Korea government (MEST) (No. 2011-0017532).

■ REFERENCES

(1) Butterfield, S. M.; Lashuel, H. A. Amyloidogenic Protein–Membrane Interactions: Mechanistic Insight from Model Systems. *Angew. Chem., Int. Ed.* **2010**, *49*, 2–29.
(2) Matthew, J. B.; Gurd, F. R.; García-Moreno, B.; Flanagan, M. A.; March, K. L.; Shire, S. J. pH-Dependent Processes in Proteins. *CRC Crit. Rev. Biochem.* **1985**, *18*, 91–197.
(3) Xiong, K.; Asciutto, E. K.; Madura, J. D.; Asher, S. A. Salt Dependence of an α-Helical Peptide Folding Energy Landscapes. *Biochemistry* **2009**, *48*, 10818–10826.
(4) Marqusee, S.; Baldwin, R. L. Helix Stabilization by Glu^{-}...Lys^{+} Salt Bridges in Short Peptides of *de novo* Design. *Proc. Natl. Acad. Sci. U. S. A.* **1987**, *84*, 8898–8902.
(5) Kao, Y.-H.; Fitch, C. A.; Bhattacharya, S.; Sarkisian, C. J.; Lecomte, J. T. J.; Garcia-Moreno, B. E. Salt Effects on Ionization Equilibria of Histidines in Myoglobin. *Biophys. J.* **2000**, *79*, 1637–1654.
(6) Khandogin, J.; Chen, J.; Brooks, C. L., III Exploring Atomistic Details of pH-Dependent Peptide Folding. *Proc. Natl. Acad. Sci. U. S. A.* **2006**, *103*, 18546–18550.
(7) Feng, J.; Wong, K.-Y.; Lynch, G. C.; Gao, X.; Pettitt, B. M. Salt Effects on Surface -Tethered Peptides in Solution. *J. Phys. Chem. B* **2009**, *113*, 9472–9478.
(8) Ozbas, B.; Kretsinger, J.; Rajagopal, K.; Schneider, J. P.; Pochan, D. J. Salt-Triggered Peptide Folding and Consequent Self-Assembly into Hydrogels with Tunable Modulus. *Macromolecules* **2004**, *37*, 7331–7337.
(9) Majd, S.; Yusko, E. C.; Billeh, Y. N.; Macrae, M. X.; Yang, J.; Mayer, M. Applications of Biological Pores in Nanomedicine, Sensing, and Nanoelectronics. *Curr. Opin. Biotechnol.* **2010**, *21*, 439–76.
(10) Gu, L.-Q.; Shim, J. W. Single Molecule Sensing by Nanopores and Nanopore Devices. *Analyst* **2010**, *135*, 441–451.
(11) Kasianowicz, J. J.; Robertson, J. W. F.; Chan, E. R.; Reiner, J. E.; Stanford, V. M. Nanoscopic Porous Sensors. *Annu. Rev. Anal. Chem.* **2008**, *1*, 737–766.
(12) Bayley, H.; Luchian, T.; Shin, S.-H.; Steffensen, M. B. In *Single Molecules and Nanotechnology*; Rigler, R., Vogel, H., Eds.; Springer-Verlag: Berlin, Heidelberg, 2008; Chapter 10, pp 251–277.
(13) Wang, G.; Wang, L.; Han, Y.; Zhou, S.; Guan, X. Nanopore Stochastic Detection: Diversity, Sensitivity, and Beyond. *Acc. Chem. Res.* **2013**, *46*, 2867–2877.
(14) Movileanu, L. Interrogating Single Proteins through Nanopores: Challenges and Opportunities. *Trends Biotechnol.* **2009**, *27*, 333–341.
(15) Dekker, C. Solid-State Nanopores. *Nat. Nanotechnol.* **2007**, *2*, 209–215.
(16) Oukhaled, A.; Bacri, L.; Pastoriza-Gallego, M.; Betton, J.-M.; Pelta, J. Sensing Proteins through Nanopores: Fundamental to Applications. *ACS Chem. Biol.* **2012**, *7*, 1935–1949.
(17) Bezrukov, S. M.; Vodyanoy, I.; Parsegian, V. A. Counting Polymers Moving through a Single-Ion Channel. *Nature* **1994**, *370*, 279–281.
(18) Kasianowicz, J. J.; Brandin, E.; Branton, D.; Deamer, D. W. Characterization of Individual Polynucleotide Molecules Using a

Membrane Channel. *Proc. Natl. Acad. Sci. U. S. A.* **1996**, *93*, 13770−13773.
(19) Luchian, T.; Shin, S.-H.; Bayley, H. Single-Molecule Covalent Chemistry with Spatially Separated Reactants. *Angew. Chem., Int. Ed.* **2003**, *42*, 3766−3771.
(20) Luchian, T.; Shin, S.-H.; Bayley, H. Kinetics of a Three-Step Reaction Observed at the Single Molecule Level. *Angew. Chem., Int. Ed.* **2003a**, *42*, 1926−1929.
(21) Shin, S.−H.; Luchian, T.; Cheley, S.; Braha, O.; Bayley, H. Kinetics of a Reversible Covalent−Bond Forming Reaction Observed at the Single Molecule Level. *Angew. Chem., Int. Ed.* **2002**, *41*, 3707−3709.
(22) Gu, L.-Q.; Braha, O.; Conlan, S.; Cheley, S.; Bayley, H. Stochastic Sensing of Organic Analytes by a Pore-Forming Protein Containing a Molecular Adapter. *Nature* **1999**, *398*, 686−690.
(23) Asandei, A.; Mereuta, L.; Luchian, T. The Kinetics of Ampicillin Complexation by γ Cyclodextrins. A Single Molecule Approach. *J. Phys. Chem. B* **2011**, *115*, 10173−10181.
(24) Asandei, A.; Apetrei, A.; Luchian, T. Uni-Molecular Detection and Quantification of Selected β-Lactam Antibiotics with a Hybrid α - Hemolysin Protein Pore. *J. Mol. Recognit.* **2011**, *24*, 199−207.
(25) Reiner, J. E.; Kasianowicz, J. J.; Nablo, B. J.; Robertson, J. W. F. Theory for Polymer Analysis Using Nanopore-Based Single-Molecule Mass Spectrometry. *Proc. Natl. Acad. Sci. U. S. A.* **2010**, *107*, 12080−12085.
(26) Robertson, J. W. F.; Rodrigues, C. G.; Stanford, V. M.; Rubinson, K. A.; Krasilnikov, O. V.; Kasianowicz, J. J. Single-Molecule Mass Spectrometry in Solution Using a Solitary Nanopore. *Proc. Natl. Acad. Sci. U. S. A.* **2007**, *104*, 8207−8211.
(27) Cressiot, B.; Oukhaled, A.; Patriarche, G.; Pastoriza-Gallego, M.; Betton, J.-M.; Auvray, L.; Muthukumar, M.; Bacri, L.; Pelta, J. Protein Transport through a Narrow Solid-State Nanopore at High Voltage: Experiments and Theory. *ACS Nano* **2012**, *6*, 6236−6243.
(28) Merstorf, C.; Cressiot, B.; Pastoriza-Gallego, M.; Oukhaled, A.; Betton, J.-M.; Auvray, L.; Pelta, J. Wild Type, Mutant Protein Unfolding and Phase Transition Detected by Single-Nanopore Recording. *ACS Chem. Biol.* **2012**, *7*, 652−658.
(29) Oukhaled, G.; Mathé, J.; Biance, A.-L.; Bacri, L.; Betton, J.-M.; Lairez, D.; Pelta, J.; Auvray, L. Unfolding of Proteins and Long Transient Conformations Detected by Single Nanopore Recording. *Phys. Rev. Lett.* **2007**, *98*, 158101.
(30) Talaga, D. S.; Li, J. Single-Molecule Protein Unfolding in Solid State Nanopores. *J. Am. Chem. Soc.* **2009**, *131*, 9287−9297.
(31) Freedman, K. J.; Jürgens, M.; Prabhu, A.; Ahn, C. W.; Jemth, P.; Edel, J. B.; Kim, M. J. Chemical, Thermal, and Electric Field Induced Unfolding of Single Protein Molecules Studied Using Nanopores. *Anal. Chem.* **2011**, *83*, 5137−5144.
(32) Pastoriza-Gallego, M.; Gibrat, G.; Thiebot, B.; Betton, J.-M.; Pelta, J. Polyelectrolyte and Unfolded Protein Pore Entrance Depends on the Pore Geometry. *Biochim. Biophys. Acta* **2009**, *1788*, 1377−1386.
(33) Payet, L.; Martinho, M.; Pastoriza-Gallego, M.; Betton, J.-M.; Auvray, L.; Pelta, J.; Mathé, J. Thermal Unfolding of Proteins Probed at the Single Molecule Level Using Nanopores. *Anal. Chem.* **2012**, *84*, 4071−4076.
(34) Oukhaled, A.; Cressiot, B.; Bacri, L.; Pastoriza-Gallego, M.; Betton, J.-M.; Bourhis, E.; Jede, R.; Gierak, J.; Auvray, L.; Pelta, J. Dynamics of Completely Unfolded and Native Proteins through Solid-State Nanopores as a Function of Electric Driving Force. *ACS Nano* **2011**, *5*, 3628−3638.
(35) Freedman, K. J.; Haq, S. R.; Edel, J. B.; Jemth, P.; Kim, M. J. Single Molecule Unfolding and Stretching of Protein Domains Inside a Solid-State Nanopore by Electric Field. *Sci. Rep.* **2013**, *3*, 1638.
(36) Song, L.; Hobaugh, M. R.; Shustak, C.; Cheley, S.; Bayley, H.; Gouaux, J. E. Structure of Staphylococcal Alpha-Hemolysin, a Heptameric Transmembrane Pore. *Science* **1996**, *274*, 1859−1866.
(37) Bezrukov, S. M.; Kasianowicz, J. J. The Charge State of an Ion Channel Controls Neutral Polymer Entry into its Pore. *Eur. Biophys. J.* **1997**, *26*, 471−476.
(38) Kang, X.-F.; Gu, L.-Q.; Cheley, S.; Bayley, H. Single Protein Pores Containing Molecular Adapters at High Temperatures. *Angew. Chem., Int. Ed.* **2005**, *44*, 1495−1499.
(39) Oukhaled, G.; Bacri, L.; Mathé, J.; Pelta, J.; Auvray, L. Effect of Screening on the Transport of Polyelectrolytes through Nanopores. *Europhys. Lett.* **2008**, *82*, 48003.
(40) Rodriguez-Larrea, D.; Bayley, H. Multistep Protein Unfolding during Nanopore Translocation. *Nat. Nanotechnol.* **2013**, *8*, 288−295.
(41) Jeon, B.; Muthukumar, M. Polymer Capture by α-Hemolysin Pore upon Salt Concentration Gradient. *J. Chem. Phys.* **2014**, *140*, 015101.
(42) Movileanu, L.; Schmittschmitt, J.; Scholtz, J. M.; Bayley, H. Interaction of Peptides with a Protein Nanopore. *Biophys. J.* **2005**, *89*, 1030−1045.
(43) Asandei, A.; Apetrei, A.; Park, Y.; Hahm, K.-S.; Luchian, T. Investigation of Single-Molecule Kinetics Mediated by Weak Hydrogen-Bonds within a Biological Nanopore. *Langmuir* **2011**, *27*, 19−24.
(44) Stefureac, R.; Long, Y.; Kraatz, H. B.; Howard, P.; Lee, J. S. Transport of α-Helical Peptides through α - Hemolysin and Aerolysin Pores. *Biochemistry* **2006**, *45*, 9172−9179.
(45) Wolfe, A. J.; Mohammad, M. M.; Cheley, S.; Bayley, H.; Movileanu, L. Catalyzing the Translocation of Polypeptides through Attractive Interactions. *J. Am. Chem. Soc.* **2007**, *129*, 14034−14041.
(46) Goodrich, C. P.; Kirmizialtin, S.; Huyghues-Despointes, B. M.; Zhu, A.; Scholtz, J. M.; Makarov, D. E.; Movileanu, L. Single-Molecule Electrophoresis of Beta-Hairpin Peptides by Electrical Recordings and Langevin Dynamics Simulations. *J. Phys. Chem. B* **2007**, *111*, 3332−3335.
(47) Mohammad, M. M.; Prakash, S.; Matouschek, A.; Movileanu, L. Controlling a Single Protein in a Nanopore through Electrostatic Traps. *J. Am. Chem. Soc.* **2008**, *130*, 4081−4088.
(48) Mereuta, L.; Schiopu, I.; Asandei, A.; Park, Y.; Hahm, K. S.; Luchian, T. Protein Nanopore-Based, Single-Molecule Exploration of Copper Binding to an Antimicrobial-Derived, Histidine-Containing Chimera Peptide. *Langmuir* **2012**, *28*, 17079−17091.
(49) Wang, G.; Wang, L.; Han, Y.; Zhou, S.; Guan, X. Nanopore Detection of Copper Ions Using a Polyhistidine Probe. *Biosens. Bioelectron.* **2014**, *53*, 453−458.
(50) Asandei, A.; Schiopu, I.; Iftemi, S.; Mereuta, L.; Luchian, T. Investigation of Cu^{2+} Binding to Human and Rat Amyloid Fragments Aβ (1−16) with a Protein Nanopore. *Langmuir* **2013**, *29*, 15634−15642.
(51) Asandei, A.; Iftemi, S.; Mereuta, L.; Schiopu, I.; Luchian, T. Probing of Various Physiologically Relevant Metals-Amyloid-β Peptide Interactions with a Lipid Membrane-Immobilized Protein Nanopore. *J. Membr. Biol.* **2014**, *247*, 523−530.
(52) Baran, C.; Smith, G. S.; Bamm, V. V.; Harauz, G.; Lee, J. S. Divalent Cations Induce a Compaction of Intrinsically Disordered Myelin Basic Protein. *Biochem. Biophys. Res. Commun.* **2010**, *391*, 224−229.
(53) Stefureac, R.; Waldner, L.; Howard, P.; Lee, J. S. Nanopore Analysis of a Small 86-Residue Protein. *Small* **2008**, *4*, 59−63.
(54) Wang, H.-Y.; Ying, Y.-L.; Li, Y.; Kraatz, H.-B.; Long, Y.-T. Nanopore Analysis of β-Amyloid Peptide Aggregation Transition Induced by Small Molecules. *Anal. Chem.* **2011**, *83*, 1746−1752.
(55) Mereuta, L.; Roy, M.; Asandei, A.; Lee, J. K.; Park, Y.; Andricioaei, I.; Luchian, T. Slowing Down Single-Molecule Trafficking through a Protein Nanopore Reveals Intermediates for Peptide Translocation. *Sci. Rep.* **2014**, *4*, 3885.
(56) Sandberg, A.; Luheshi, L. M.; Söllvander, S.; Pereira de Barros, T.; Macao, B.; Knowles, T. P.; Biversta, H.; Lendel, C.; Ekholm-Petterson, F.; Dubnovitsky, A.; Lannfelt, L.; Dobson, C. M.; Hard, T. Stabilization of Neurotoxic Alzheimer Amyloid-β Oligomers by Protein Engineering. *Proc. Natl. Acad. Sci. U. S. A.* **2010**, *107*, 15595−15600.
(57) Abelein, A.; Abrahams, J. P.; Danielsson, J.; Gräslund, A.; Jarvet, J.; Luo, J.; Tiiman, A.; Wärmländer, S. K. T. S. The Hairpin Conformation of the Amyloid β Peptide Is an Important Structural

Motif along the Aggregation Pathway. *J. Biol. Inorg. Chem.* **2014**, *19*, 623−634.
(58) Liao, S.-M.; Du, Q.-S.; Meng, J.-Z.; Pang, Z.-W.; Huang, R.-B. The Multiple Roles of Histidine in Protein Interactions. *Chem. Cent. J.* **2013**, *7*, 44.
(59) Lee, D. G.; Park, Y.; Jin, I.; Hahm, K. S.; Lee, H. H.; Moon, Y. H.; Woo, E. R. Structure−Antiviral Activity Relationships of Cecropin A-Magainin 2 Hybrid Peptide and its Analogues. *J. Pept. Sci.* **2004**, *10*, 298−303.
(60) Further information can be found at the following GenScriptWeb site: https://www.genscript.com/ssl-bin/site2/peptide_calculation.cgi (accessed April 5, 2014).
(61) DeBlois, R. W.; Bean, C. P. Counting and Sizing of Submicron Particles by the Resistive Pulse Technique. *Rev. Sci. Instrum.* **1970**, *41*, 909−916.
(62) Yusko, E. C.; Johnson, J. M.; Majd, S.; Prangkio, P.; Rollings, R. C.; Li, J.; Yang, J.; Mayer, M. Controlling Protein Translocation Through Nanopores with Bio-Inspired Fluid Walls. *Nat. Nanotechnol.* **2011**, *6*, 253−260.
(63) Wong, C. T. A.; Muthukumar, M. Polymer Translocation through α- Hemolysin Pore with Tunable Polymer-Pore Electrostatic Interaction. *J. Chem. Phys.* **2010**, *133*, 045101.
(64) Wanunu, M.; Morrison, W.; Rabin, Y.; Grosberg, A. Y.; Meller, A. Electrostatic Focusing of Unlabeled DNA into Nanoscale Pores using a Salt Gradient. *Nat. Nanotechnol.* **2010**, *5*, 160−165.
(65) Stein, D.; Kruithof, M.; Dekker, C. Surface-Charge-Governed Ion Transport in Nanofluidic Channels. *Phys. Rev. Lett.* **2004**, *93*, 035901.
(66) Chang, H.; Kosari, F.; Andreadakis, G.; Alam, M. A.; Vasmatzis, G.; Bashir, R. DNA-Mediated Fluctuations in Ionic Current through Silicon Oxide Nanopore Channels. *Nano Lett.* **2004**, *4*, 1551−1556.
(67) Garcia-Mira, M. M.; Sadqi, M.; Fischer, N.; Sanchez-Ruiz, J. M.; Munoz, V. Experimental Identification of Downhill Protein Folding. *Science* **2002**, *298*, 2191−2195.
(68) Arbely, E.; Rutherford, T. J.; Sharpe, T. D.; Ferguson, N.; Fersht, A. R. Downhill versus Barrier-Limited Folding of BBL 1: Energetic and Structural Perturbation Effects upon Protonation of a Histidine of Unusually Low pKa. *J. Mol. Biol.* **2009**, *387*, 986−992.
(69) Bostrom, M.; Williams, D. R. M.; Ninham, B. W. Specific Ion Effects: Why the Properties of Lysozyme in Salt Solutions Follow a Hofmeister Series. *Biophys. J.* **2003**, *85*, 686−694.
(70) Rosenstein, J. K.; Wanunu, M.; Merchant, C. A.; Drndić, M.; Shepard, K. L. Integrated Nanopore Sensing Platform with Sub-Microsecond Temporal Resolution. *Nat. Methods* **2012**, *9*, 487−492.